DOI: 10.48011/asba.v2i1.1519

Sinusoidal PWM Techniques in Rotor Pole Segmentation to Reduce Permanent Magnet Synchronous Machine Torque Ripple ⋆

Khristian M. de Andrade Jr., Hugo E. Santos, Wellington M. Vilela, Geyverson T. de Paula

School of Electrical, Mechanical and Computer Engineering, Federal University of Goiás, Goiânia, GO 74605-010 BR, (e-mails: khristianjr11@gmail.com, hes.ufgee@gmail.com, wmisaelvilela@gmail.com, geyverson@gmail.com).

Abstract: Torque ripples can cause mechanical stress in electrical machines, among other problems. The present paper proposes three methods to reduce these ripples in the permanent magnets synchronous machine considering rotor poles design. These methods consist in segmenting the rotor poles, with width and distances between segments obtained by Sinusoial PWM techniques. The modulating wave is a sinwave which has the same frequency as the airgap flux density fundamental harmonic. Method 1 contemplates the unipolar SPWM technique, whereas methods 1 and 2 used the bipolar SWPM technique. Furthermore, the equations used to predict the cogging torque behavior are presented and verified by means of a finite element analysis. The torque ripple reduction is achieved due to the elimination of back-electromotive force harmonics and the decrease in the cogging torque peak. Method 1 has proved to be the most effective, reducing the torque ripple by 51.38% and 76.61% for the 4-pole and 8-pole machines, respectively. In addition, the magnet volume utilized has been reduced by 22.55% for the 4-pole machine, but the average torque value has been reduced by 18.7%. It is worth mentioning that the proposed methods do not require skewing to reduce the torque ripple.

Keywords: pole segmentation, Sinusoidal PWM, surface mounted PMSM, torque ripple reduction

1. INTRODUCTION

Permanent magnet (PM) synchronous motors (SM) are being used worldwide in traction applications due to to their high energy density, low inertia, easy control and low maintenance (Sulaiman et al., 2011a). However, this type of machine has undesired torque pulsations caused by the cogging torque and the interaction of armature current harmonics with the PM flux-linkage harmonics, and, consequently, with the back-electromotive force (back-emf). These pulsations cause noise, vibration and losses. Therefore, they should be mitigated to improve the performance of the machine.

Numerous techniques have been developed to reduce cogging torque and torque ripple (Miller and Hendersot, 1995; Sulaiman et al., 2011b; Ishikawa and Slemon, 1993; Xintong et al., 2009; Sang-Moon Hwang et al., 2001; Chang Seop Koh and Jin-Soo Seol, 2003; Gao et al., 2017; Lateb et al., 2006; Ashabani and Mohamed, 2011; Chaithongsuk et al., 2009, 2010). One of the simplest is to design machines which number of slots per poles ratio is fractional (Miller and Hendersot, 1995), thus reducing the number of alignments between magnets and stator slot openings. Another technique consists in applying skewing on the magnets or stator stack lamination (Miller and Hendersot, 1995; Sulaiman et al., 2011b), preventing alignment between stator slot openings and magnets and reducing PM-linkage flux harmonics. Techniques considering variations in tooth shape have also been developed, evaluating the effects of varying tooth width, the use of teeth with different widths (Xintong et al., 2009; Sang-Moon Hwang et al., 2001) or the addition of so-called dummy slots, resulting in an effect similar to the increase in the number of slots (Sang-Moon Hwang et al., 2001; Chang Seop Koh and Jin-Soo Seol, 2003). in Gao et al. (2017), the contribution of each magnet to the total cogging torque is evaluated. The magnets which produce cogging torque in phase and those that do not are determined. Magnets that do not generate cogging torque in phase are grouped together and called "elementary cogging unit" and by shifting such units, the peak of cogging torque decreases.

Another way to reduce cogging torque is achieved by means of the rotor pole segmentation technique (Lateb et al., 2006; Ashabani and Mohamed, 2011; Chaithongsuk et al., 2009, 2010). In this technique, it is necessary to determine the number of segments, their width and the distance between them (segmentation set of variables). Analytical methods to determine the optimal values for the segmentation variables and the distance between the poles in order to minimize the first cogging torque harmonic are

⋆ All the authors would like to thank CNPq, Coordenação de Aperfeiçoamento de Pessoal de Nível Superior - Brasil (CAPES) (Finance Code 001) and FAPEG (Fundação de Amparo à Pesquisa do Estado de Goiás) for funding guarantee and support.

proposed in Lateb et al. (2006). A multi-objective optimization is performed in Ashabani and Mohamed (2011) to minimize magnet volume, cogging torque harmonics and maximize the PM flux-linkage fundamental harmonic. The optimized position of each segment that leads to the minimum cogging torque is obtained by means of the design of experiment method, considering the response surface methodology, in Abbaszadeh et al. (2011).

PWM techniques are used in Chaithongsuk et al. (2009, 2010) to perform the pole segmentation. The values for the segmentation variables are obtained by solving a non-linear system in Chaithongsuk et al. (2009) in order to eliminate specific harmonics of the PM flux-linkage. As for (Chaithongsuk et al., 2010), this set of variables is obtained using an ideal waveform for the airgap length as a modulating wave and choosing the number of pulses. The harmonics present in the PM flux-linkage are obtained for each number of pulses. Then, the number of pulses that mostly reduces the low order harmonics is chosen. The disadvantage of these methods is the presence of low-order harmonics in the back-emf after their application. In addition, the non-linear system complexity increases whereas the number of desired harmonics to be eliminated increase.

The present paper proposes the use of Sinusoidal PWM (SPWM) techniques to obtain the correct segmentation distribution and parameters, considering surface mounted permanent magnet machines (SMPMSM). Three methods are described, considering as the modulating waveform a sinusoidal waveform which frequency is the same as the fundamental frequency of the airgap flux. Differently from (Chaithongsuk et al., 2009), these proposed methods allow the elimination of all airgap flux density harmonics below certain order, working similarly to a low-pass filter. It results in a sinewave back-emf in machines with concentrated winding, the reduction of the cogging torque peak value, and thus the electromagnetic torque ripple attenuation. In addition, these methods are alternative to the skewing technique.

This paper is divided as follows. Section II describes the three developed methods to determine the pole shape using SPWM techniques. Section III describes the principles of the methods. Finally, section IV presents the results obtained via finite element analysis. All angular values mentioned throughout the paper are in mechanical degrees.

2. USAGE OF SPWM TECHNIQUES TO SHAPE ROTOR POLES

SPWM techniques generate a sequence of square pulses that emulate a sinewave by comparing the desired sinewave (the modulating waveform) and a triangular wave (the carrier). In the present paper, the modulating waveform F_m is considered to be a sinewave of amplitude A_m and frequency equal to the fundamental frequency of the airgap flux based on the machine pole number ($2p$), according to (1). The number of pole pairs is p and θ the mechanical angular position of the airgap.

$$F_m = A_m \sin(p\theta) \tag{1}$$

The modulation index, m_f, is the ratio between the carrier frequency f_c and the modulating f_m frequency, as shown in (2). As the amplitude of the modulating waveform increases above the amplitude of the carrier, the emulated waveform starts to become a square wave. Above certain value (dependent of m_f), any increase in the modulating amplitude, A_m, no longer has any effect and the emulated wave becomes completely a square wave.

$$m_f = \frac{f_c}{f_m} = \frac{2\pi f_c}{p} \tag{2}$$

In this work, two SPWM techniques are considered: the unipolar (considered in method 1) and the bipolar (considered in methods 2 and 3).

2.1 Method 1

The unipolar SPWM technique uses one carrier and two modulating waveforms, one positive and one negative. Two pulse sequences are generated, one for the positive modulating waveform and the other for the negative one. The resulting sequence is the difference between the positive and negative sequences. The pulses are generated during the instant which the carrier value is lower than the modulating ones, as illustrated in Fig. 1. This technique forces harmonics to values around the integer multiples of $2m_f$.

The method 1 consists in allocating magnets at the positions and with width defined by the pulses generated by this technique. Magnets with north pole are considered for the positive pulses and south pole for the negative ones. The resulting shape of the poles can be seen in Fig. 1 for $2\pi f_c = 8p$.

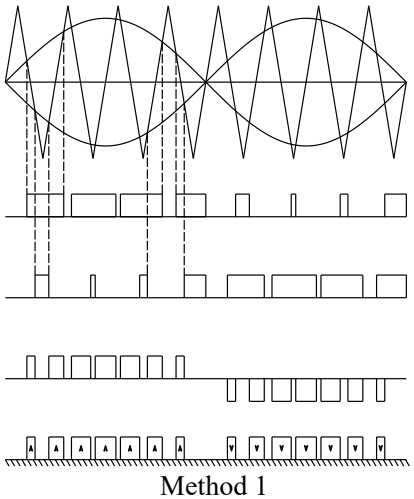

Figure 1. Unipolar SPWM (Method 1).

2.2 Methods 2 and 3

The bipolar SPWM technique uses only one modulating waveform. Like the unipolar, when the carrier value is lower than the modulating one a positive pulse is generated. Otherwise, a negative pulse is generated. This process is shown in Fig. 2. This technique forces harmonics to values around the integer multiples of m_f, thus having poorer harmonic performance when compared to the unipolar SPWM.

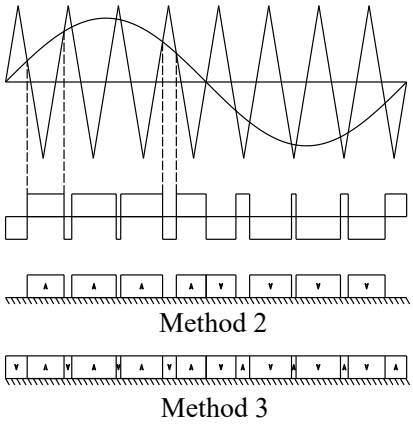

Figure 2. Bipolar SPWM (Methods 2 and 3).

The method 2 assigns a north pole magnet to each positive pulse with the same width and position in the first $\pi/2$ (electric) radians. For the rest, a south pole magnet is assigned to each negative pulse. In method 3, each positive pulse is assigned with a north pole magnet and each negative pulse with a south pole magnet. The shape of the resulting poles can be seen in Fig. 2 for $2\pi f_c = 8p$. For all three methods, empty space between segments in which the arc-span is lower than 0.2° has been filled in with magnets in order to reduce fabrication cost.

3. TORQUE RIPPLE ATTENUATION

The present section describes how the proposed methods can reduce the torque ripple of PMSM. To achieve this, the two main contributors to torque ripple in PMSMs must be attenuated. These contributors are the back-emf harmonics and the cogging torque.

3.1 Back-EMF Harmonics

s mentioned, one of the causes of the torque ripple is the interaction between harmonics of the armature current and back-emf. The back-emf low order harmonics can be eliminated through the machine design, as proposed here.

The SPWM techniques eliminate all harmonics below certain order dependent of m_f. Thus, applying these techniques to shape the poles, the low order harmonics of the back-emf are significantly reduced. In addition, the high order harmonics generated by the SPWM are filtered by the machine inductance. The result is a sinusoidal back-emf and a smooth torque.

3.2 Cogging Torque

Cogging torque arises from the tendency of the PM edges to align with the slot openings. This parasitic torque can be obtained by (3) (Lateb et al., 2006; Ashabani and Mohamed, 2011).

$$T_C(\alpha) = -\frac{\partial W(\alpha)}{\partial \alpha} = -\frac{1}{2\mu_0}\frac{\partial}{\partial \alpha}\int_V G^2(\theta)B^2(\theta,\alpha)dV \quad (3)$$

where T_C is the cogging torque, W is the no-load airgap co-energy, α is the angular position of the rotor, μ_0 the air permeability, V the airgap volume, G the relative airgap permeance and B the flux density in the middle of the airgap on a slotless machine. G is a modulating function which value is one over a tooth and zero over a slot opening. Ideally, B^2 has the same shape as of the poles, just like in Figs. 1 and 2.

Furthermore, G^2 and B^2 can be expressed by their Fourier series, as (4) and (5), respectively. G^2 has S (number of slots) cycles and B^2, $2p$ cycles for all the described methods (symmetrical poles), for a complete rotation in the airgap.

$$G^2 = \sum_{m=1}^{\infty} G_{mS}\cos(mS\theta) \quad (4)$$

$$B^2 = \sum_{k=1}^{\infty} B_{k2p}\cos[k2p(\theta-\alpha)] \quad (5)$$

The equations (4) and (5) can be applied in (3). Orthogonality properties can be employed, resulting in (6). Thus, the harmonics of G^2 and B^2 that generate cogging torque are those of order such $mS = k2p = nN_L$.

$$T_C(\alpha) = T_{C_0}\sum_{n=1}^{\infty} nN_L G_{nN_L} B_{nN_L}\sin(nN_L\alpha) \quad (6)$$

where T_{C_0} is a machine geometry-dependent constant and N_L is the LCM$(2p, S)$. The integers multiples of N_L are the harmonic orders of G^2 and B^2 that generate cogging torque.

One can notice that one way to reduce the cogging torque, the coefficients G_{nN_L} and B_{nN_L} must be reduced. G_{nN_L} can be reduced by increasing N_L, since this coefficient decreases hyperbolically with the harmonic order. It is also possible to reduce G_{nN_L} by changing the shape of teeth/slots. The pole segmentation technique can be employed to reduce B_{nN_L}.

The proposed methods forces the harmonic orders of B and B^2 to values dependent on m_f. This fact can be used to reduce the cogging torque by choosing a m_f such that to reduce the number of harmonics that generates the cogging torque. In addition, for high values of m_f, the cogging torque generating harmonics are those of higher orders, in which G_{mS} posses smaller values.

In method 1, the B^2 harmonics with highest amplitudes are those of order m_f, $m_f \pm 2$, and $m_f \pm 1$, in descending order. For methods 2 and 3, the harmonics orders $(m_f \pm 3)/2$, $(m_f \pm 1)/2$ and $(m_f \pm 5)/2$ have the highest amplitudes, listed in descending order. In order to reduce the cogging torque, one must choose a m_f such as the harmonic orders aforementioned are not multiples of $N_L/2p$. Furthermore, the higher these harmonic orders are, the smaller is the cogging torque, as mentioned.

4. FINITE ELEMENTS ANALYSIS

The proposed methods were validated by means of finite element analysis (FEA) in SMPMSMs which parameters are listed in Table 1. The PM flux-linkage, back-emf, cogging torque and electromagnetic torque were obtained varying m_f. High number of poles can make the construction of segmented pole machines unfeasible, thus the chosen pole numbers were four and eight. It is worth mentioning that all machines have no skewing either on the stator or rotor,

since the proposed methods are alternative to the skewing technique.

Table 1. Machines Parameters

Parameter	Value
Rated Power (cv)	1
Rated Speed (rpm)	1500
Number of Poles	4, 8
Inner Diameter (mm)	96
Outer Diameter (mm)	182, 132
Stack Length (mm)	102
Air gap (mm)	1
Slot Opening (mm)	2
Magnet Material	NdFeB 32 MGOe

All the obtained results were compared to reference machines with non-segmented poles. These machines can be seen in Figs. 3a and 3b. The pole pitch of these machines were optimized in order to minimize the cogging torque and keep the airgap flux density higher than 0.90 T. A 75° pole pitch was obtained for the 4-pole machine and a 30° pole pitch for the 8-pole one.

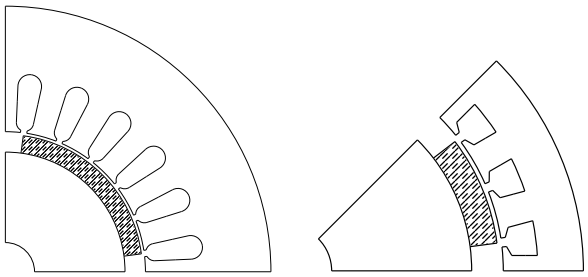

(a) 4-pole Machine (b) 8-pole Machine

Figure 3. Machines used as reference for results comparison.

The ideal and real magnetic flux density waveforms in the airgap and their spectral analysis can be seen in Figs. 4–6 for the 4-pole machine. Similar effects have been found for the 8-pole machine, therefore, their figures and analysis have been omitted. It is evident that the harmonics present in the flux for methods 1 and 3 are similar to those predicted in the section II. Method 2 uses an adaptation of bipolar SPWM, thus the presence of other harmonics besides the predicted ones is noticed. In all cases, the presence of unforeseen harmonics is also noticeable since the actual flux density is different from the ideal due to the slot openings and fringing.

The harmonics present in the airgap flux density distribution are also present in the PM flux-linkage and back-emf. It is clear that method 1 has a better harmonic performance, since for low values of m_f the back-emf harmonics generated are of high order, being filtered by the machine inductance, thus reducing torque ripple.

The back-emf harmonics for all three methods and the reference 4-pole machine can be seen in Fig. 7 for $m_f = 15$. These waveforms were normalized by their respective peak value. One can notice that method 1 has the most sinewave-like waveform, showing the best harmonic performance. In addition, methods 2 and 3 present waveforms similar to the reference one since the SPWM generates low order harmonics for this value of m_f.

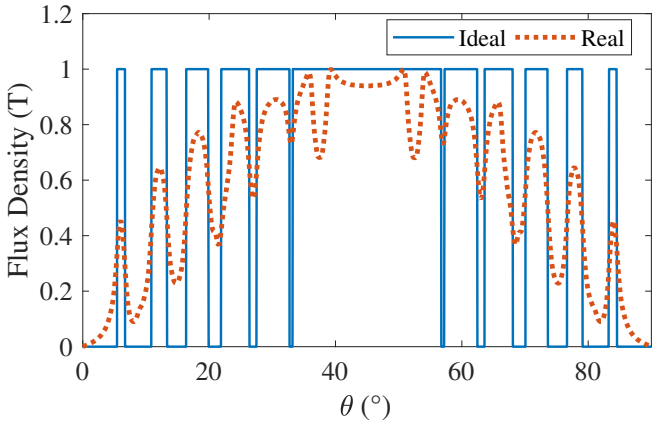

(a) Ideal and Real flux density in the airgap middle.

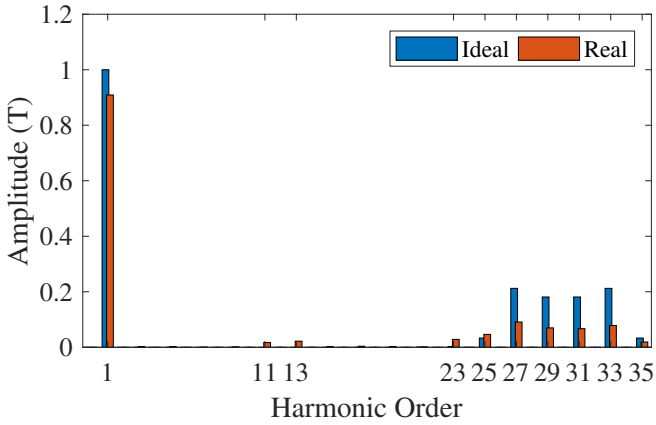

(b) Harmonics present in the flux density the airgap middle.

Figure 4. Method 1 flux density in the airgap middle (4-pole machine).

Although discarding distances smaller than 0.2° had no significant effects on the 4-pole machine, for high values of m_f, this constraint interferes in the output parameters of the 8-pole machine. This way, the back-emf waveforms of all three methods and 8-pole reference machine, as presented in Fig. 8 for $m_f = 25$, are no longer similar to a sinewave.

The magnetic flux density first harmonic suffers variations when segmenting the poles. This can reduce the PM flux linkage, back-emf and, consequently, the average electromagnetic torque. The PM flux linkage variations when using the proposed methods can be seen in Figs. 9 and 10. Values of m_f lower than six results in a great reduction the magnetic flux, thus they must not be used. A reduction by about 24% and by 5% respectively for the 4-pole and 8-pole machines is observed. Method 2 has a higher magnetic flux density first harmonic, as can be seen in Fig. 5b, thus it presents a PM flux linkage about 20% higher than the other methods.

Both the 4-pole and 8-pole machines have $N_L = 24$. Thus, those harmonic orders presented in Section III must not be multiples of 6 and 3 for the 4-pole and 8-pole machines, respectively. The cogging torque peak values can be seen in Figs. 11 and 12.

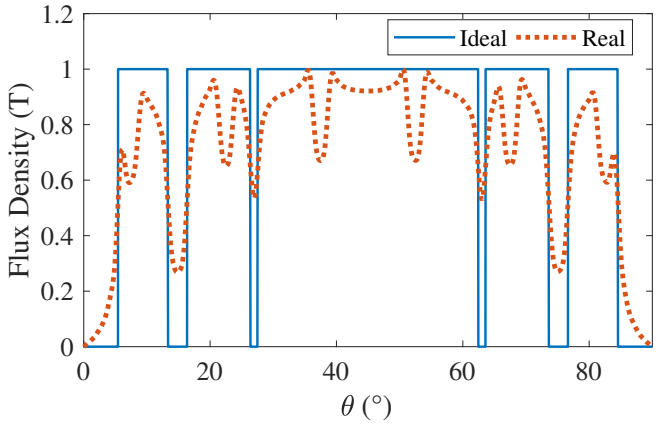

(a) Ideal and Real flux density in the middle of the airgap.

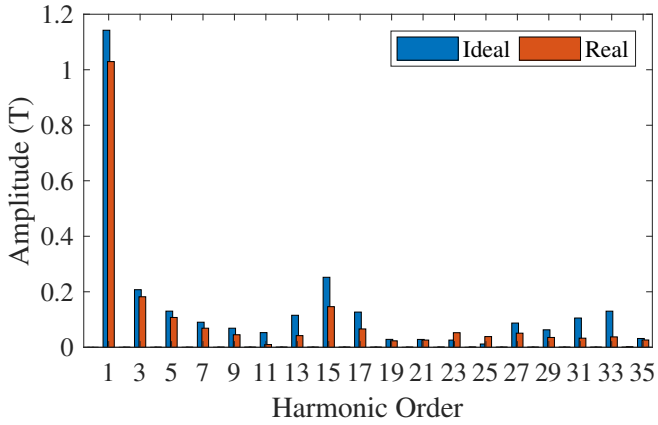

(b) Harmonics present in the flux density in the middle of the airgap.

Figure 5. Method 2 flux density in the middle of the air gap (4-pole machine).

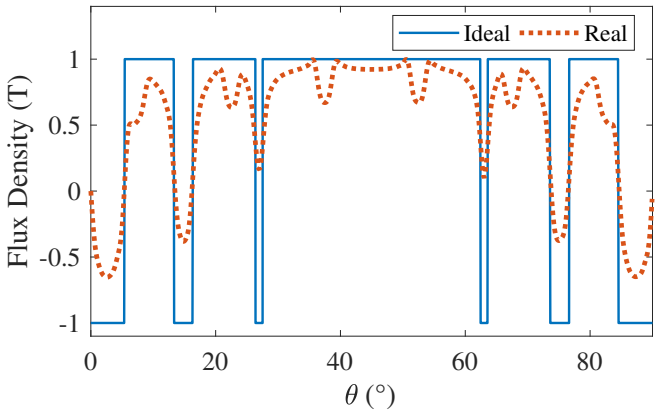

(a) Ideal and Real flux density in the middle of the airgap.

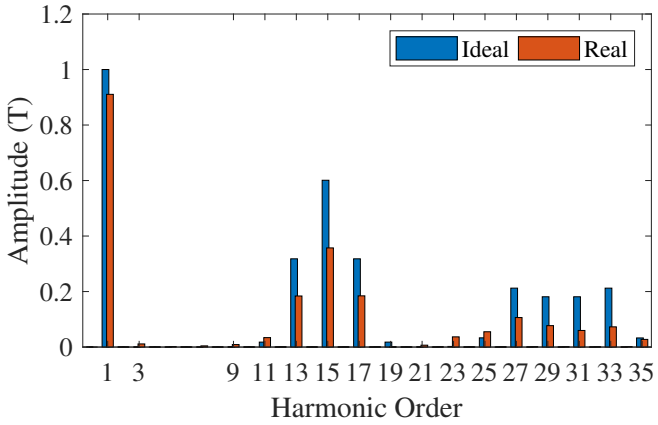

(b) Harmonics present in the flux density the middle of the airgap.

Figure 6. Method 3 flux density in the middle of the air gap (4-pole machine).

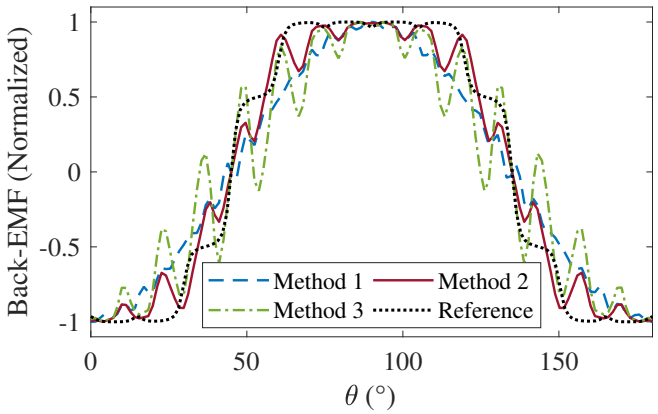

Figure 7. Back-EMF comparison for the 4-pole machine with $m_f = 15$.

In the 4-pole machine using method 1, the cogging torque has high values if m_f is even, specially multiple of 6. This occurs since $mf \pm 2$ or m_f is a multiple of 6 for even m_f values. The 8-pole machine has higher cogging torque values since m_f, $m_f \pm 2$ or $m_f \pm 1$ is a multiple of 3 regardless the m_f value. Since the $m_f \pm 1$ harmonics have the smallest amplitudes, when they are multiple of 3 the cogging torque has the smallest values in the 8-pole machine. Method 1 reduces the cogging torque by up to 59.28% and 78.54% for the 4-pole and 8-pole machines, respectively.

Now, for all machines using either method 2 or 3, for odd m_f values, specially those multiple of 3, the cogging torque is high. This occurs since for odd m_f values, $(m_f \pm 1)/2$, $(m_f \pm 3)/2$ or $(m_f \pm 5)/2$ is either multiple of 3 or 6. Method 3 presents better results than method 2, reducing the cogging torque by up to 42.79% and 77% for the 4-pole and 8-pole machines, respectively.

The variations in the torque average value can be seen in Figs. 13 and 14. To obtain the electromagnetic torque the machines were considered having an ideal sinusoidal drive with a peak current of 2.8 A. A similar pattern to the PM flux-linkage is observed, the difference is caused by the saturation level of the machine. A reduction by about 18.7% and 7% respectively for the 4-pole and 8-pole machines is observed. Again, method 2 presents the highest average torque between the three methods, about 10% higher, thanks to its higher flux density first harmonic.

It is recommended by (IEEE, Accessed 18 Sep. 2019) that the electromagnetic torque ripple is obtained by (7). This value is obtained for all methods and the reference machines and shown in Figs. 15 and 16. One can notice the

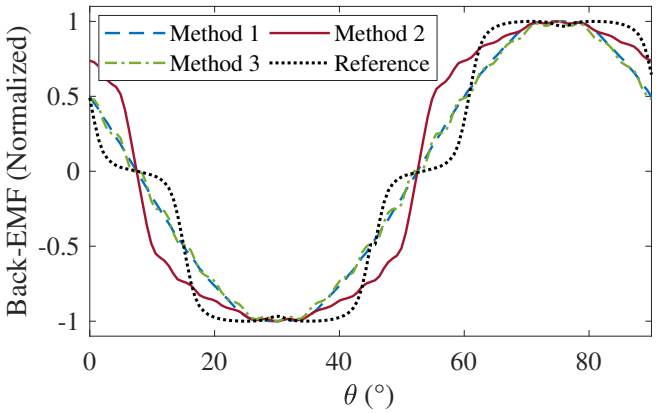

Figure 8. Back-EMF comparison for the 8-pole machine with $m_f = 25$.

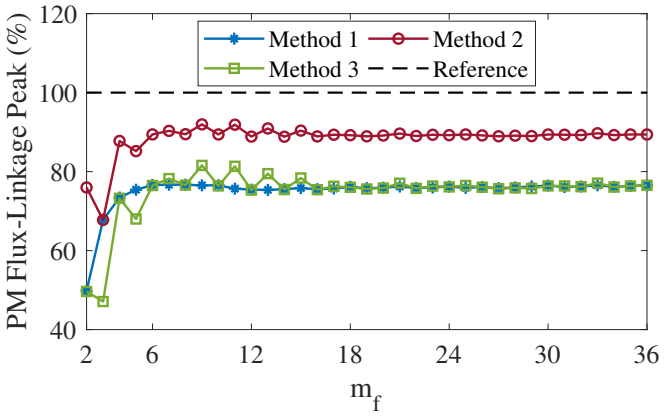

Figure 9. PM Flux-linkage peak value comparison for the 4-pole machine.

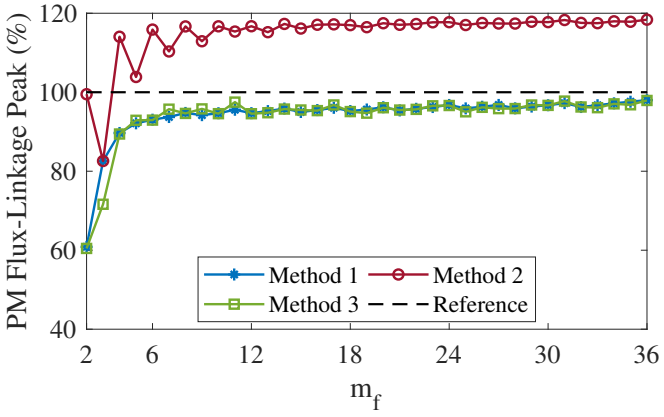

Figure 10. PM Flux-linkage peak value comparison for the 8-pole machine.

similarities between the torque ripple curves and cogging torque ones. As m_f increases this is more noticeable, since the back-emf harmonic frequencies increases proportionally, being filtered by the inductance of the machine. This occurs since the cogging and electromagnetic torques have the same magnitude for these machines. Method 1 presents the best results, reducing the torque ripple by up to 51.38% for the 4-pole machine and 76.61% for the 8-pole one.

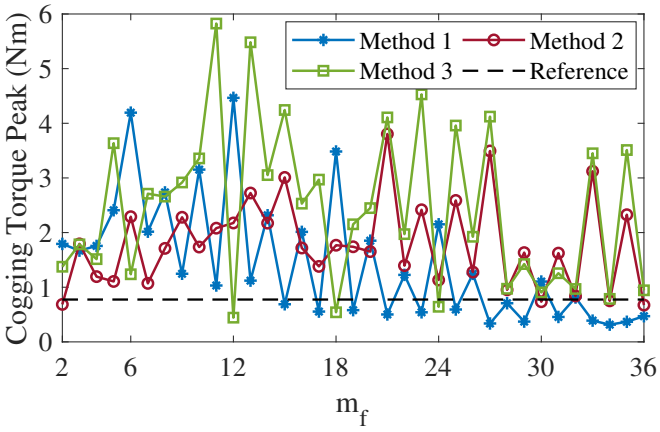

Figure 11. Cogging torque peak value comparison for the 4-pole machine.

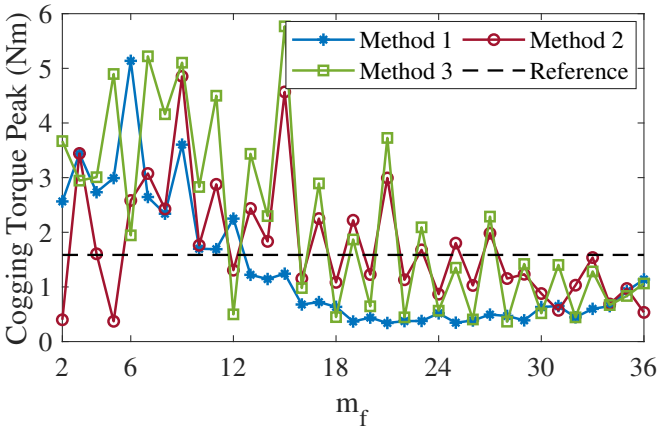

Figure 12. Cogging torque peak value comparison for the 8-pole machine.

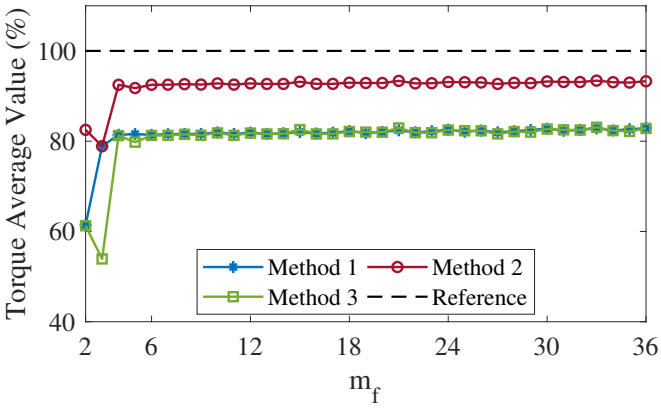

Figure 13. Torque average value comparison for the 4-pole machine.

$$T_r\,(\%) = \frac{\max(T) - \min(T)}{2\,\mathrm{avg}(T)} 100\% \qquad (7)$$

where T_r is the torque ripple and T the electromagnetic torque.

Electromagnetic torque waveforms for $m_f = 15$ can be seen in Figs. 17 and 18. It is possible to notice the reduction both in the average and ripple values when using the methods for method 1. It it also possible to observe that

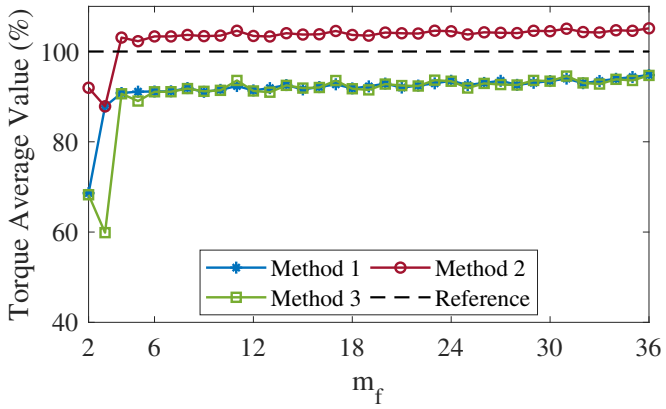

Figure 14. Torque average value comparison for the 8-pole machine.

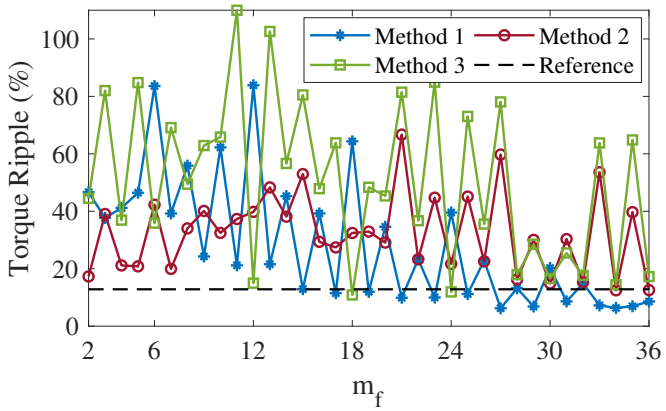

Figure 15. Torque ripple comparison for the 4-pole machine.

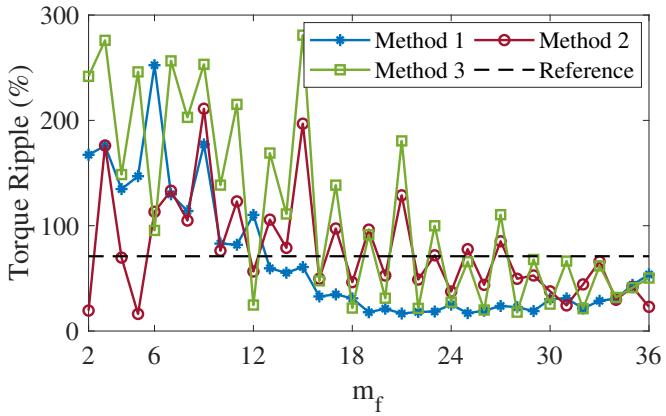

Figure 16. Torque ripple comparison for the 8-pole machine.

the chosen m_f caused an increase in the ripple for methods 2 and 3.

Values of m_f lower than 25 guarantee the machine construction feasibility. Values higher than this threshold produce PM segments with width inferior to 0.22°.

In terms of PM volume, methods 2 and 3 present no advantages, as can be noted through Figs. 19 and 20. Method 1 reduces the PM volume by about 22.55% and 3.28% for the 4-pole and 8-pole machines, respectively,

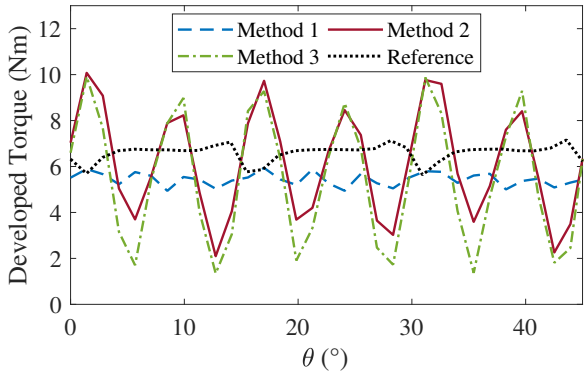

Figure 17. Torque waveforms for the 4-pole machine and $m_f = 15$.

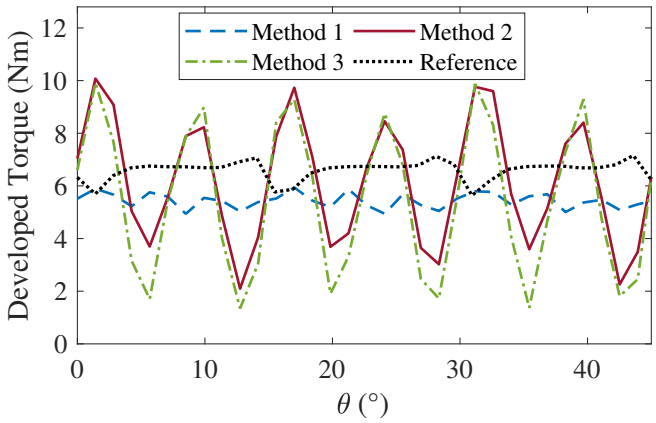

Figure 18. Torque waveforms for the 4-pole machine and $m_f = 15$.

for values of m_f lower than 25. Techniques in which the cogging torque is minimized by optimizing the pole shape (Sculiller, 2014; Sun and Wang, 2019; Lukaniszyn et al., 2004; Shin et al., 2009) may lead to no PM volume reduction when compared to method 1. Furthermore, pole shape optimizing techniques demand high computational effort and the resulting PM shape or distribution can be hard to manufacture/implement.

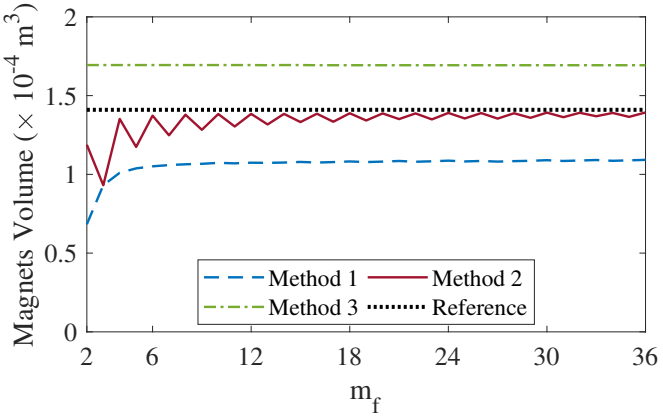

Figure 19. Magnets volume comparison (4-pole machine).

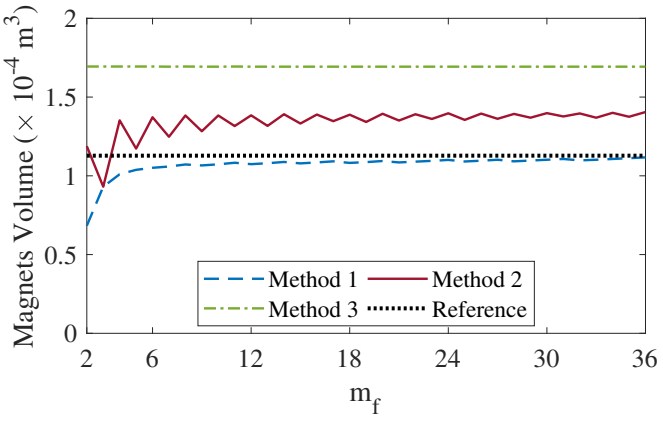

Figure 20. Magnets volume comparison (8-pole machine).

5. CONCLUSION

The described methods for reducing the electromagnetic torque ripple consider the rotor pole segmentation, being the width and distance between the segments provided by SPWM (unipolar or bipolar) techniques. The methods are easy to implement, require low computational effort to obtain the desired waveform and allow the reduction of the cogging torque and elimination of back-emf harmonics. Method 1 presents the best results, reducing the torque ripple by 76.61% for the 8-pole machine and by 51.38% for the 4-pole one. In addition, method 1 reduces the PM volume by 22.55% at the cost of a 18.7% loss in the electromagnetic torque of the 4-pole machine. It should be emphasized that the results of the methods depend strongly on m_f. Its value can reduce or increase the cogging torque. Considering the machine construction feasibility, m_f values below 25 are indicated for all methods and machines considered. Although the construction feasibility of the 8-pole machine is guaranteed for this values, the resulting back-emf for m_f values higher than 15 is more similar to a trapezoidal waveform, since distances smaller than 0.2° are discarded.

REFERENCES

Abbaszadeh, K., Alam, F., and S.A.Saied (2011). Cogging torque optimization in surface-mounted permanent-magnet motors by using design of experiment. *Elsevier Energy Conversion and Management*, 52(10), 3075–3082.

Ashabani, M. and Mohamed, Y.A.I. (2011). Multiobjective shape optimization of segmented pole permanent-magnet synchronous machines with improved torque characteristics. *IEEE Transactions on Magnetics*, 47(4), 795–804.

Chaithongsuk, S., Takorabet, N., and Meibody-Tabar, F. (2009). On the use of pulse width modulation method for the elimination of flux density harmonics in the air-gap of surface pm motors. *IEEE Transactions on Magnetics*, 45(3), 1736–1739.

Chaithongsuk, S., Takorabet, N., Nahid-Mobarakeh, B., and Meibody-Tabar, F. (2010). Optimal design of pm motors for quasi-sinusoidal air-gap flux density. In *45th International Universities Power Engineering Conference UPEC2010*, 1–6.

Chang Seop Koh and Jin-Soo Seol (2003). New cogging-torque reduction method for brushless permanent-magnet motors. *IEEE Transactions on Magnetics*, 39(6), 3503–3506.

Gao, J., Wang, G., Liu, X., Zhang, W., Huang, S., and Li, H. (2017). Cogging torque reduction by elementary-cogging-unit shift for permanent magnet machines. *IEEE Transactions on Magnetics*, 53(11), 1–5.

IEEE (Accessed 18 Sep. 2019). *IEEE 1812-2014 - IEEE Trial-Use Guide for Testing Permanent Magnet Machines*. URL `https://standards.ieee.org/standard/1812-2014.html`.

Ishikawa, T. and Slemon, G.R. (1993). A method of reducing ripple torque in permanent magnet motors without skewing. *IEEE Transactions on Magnetics*, 29(2), 2028–2031.

Lateb, R., Takorabet, N., and Meibody-Tabar, F. (2006). Effect of magnet segmentation on the cogging torque in surface-mounted permanent-magnet motors. *IEEE Transactions on Magnetics*, 42(3), 442–445.

Lukaniszyn, M., JagieLa, M., and Wrobel, R. (2004). Optimization of permanent magnet shape for minimum cogging torque using a genetic algorithm. *IEEE Transactions on Magnetics*, 40(2), 1228–1231.

Miller, T.J.E. and Hendersot, J.R. (1995). *Design of Brushless Permanent- Magnet Motors*. Oxford Univ. Press, London, U.K., 2 edition.

Sang-Moon Hwang, Jae-Boo Eom, Yoong-Ho Jung, Deug-Woo Lee, and Beom-Soo Kang (2001). Various design techniques to reduce cogging torque by controlling energy variation in permanent magnet motors. *IEEE Transactions on Magnetics*, 37(4), 2806–2809.

Scuiller, F. (2014). Magnet shape optimization to reduce pulsating torque for a five-phase permanent-magnet low-speed machine. *IEEE Transactions on Magnetics*, 50(4), 1–9.

Shin, P.S., Woo, S.H., and Koh, C.S. (2009). An optimal design of large scale permanent magnet pole shape using adaptive response surface method with latin hypercube sampling strategy. *IEEE Transactions on Magnetics*, 45(3), 1214–1217.

Sulaiman, E., Kosaka, T., and Matsui, N. (2011a). High power density design of 6-slot–8-pole hybrid excitation flux switching machine for hybrid electric vehicles. *IEEE Transactions on Magnetics*, 47(10), 4453–4456.

Sulaiman, E., Kosaka, T., and Matsui, N. (2011b). High power density design of 6-slot–8-pole hybrid excitation flux switching machine for hybrid electric vehicles. *IEEE Transactions on Magnetics*, 47(10), 4453–4456.

Sun, H.Y. and Wang, K. (2019). Effect of third harmonic flux density on cogging torque in surface-mounted permanent magnet machines. *IEEE Transactions on Industrial Electronics*, 66(8), 6150–6158.

Xintong, J., Jingwei, X., Yong, L., and Yongping, L. (2009). Theoretical and simulation analysis of influences of stator tooth width on cogging torque of bldc motors. *IEEE Transactions on Magnetics*, 45(10), 4601–4604.